

# Strong-Coupling Lattice QCD on Anisotropic Lattices

Philippe de Forcrand<sup>\*a,b</sup>, Wolfgang Unger<sup>†c</sup>, and Hélvio Vairinhos<sup>‡</sup>

<sup>a</sup>*Institut für Theoretische Physik, ETH Zürich, CH-8093 Zürich, Switzerland*

<sup>b</sup>*CERN, TH Division, CH-1211 Geneva 23, Switzerland*

<sup>c</sup>*Fakultät für Physik, Universität Bielefeld, Universitätstraße 25, D33619 Bielefeld, Germany*

## Abstract

Anisotropic lattice spacings are mandatory to reach the high temperatures where chiral symmetry is restored in the strong coupling limit of lattice QCD. Here, we propose a simple criterion for the nonperturbative renormalisation of the anisotropy coupling  $\gamma$  in strongly-coupled  $SU(N_c)$  or  $U(N_c)$  lattice QCD with massless staggered fermions. We then compute the renormalised anisotropy  $\xi(\gamma)$ , and the strong-coupling analogue of Karsch's coefficients (the running anisotropy), for  $N_c = 3$ . We achieve high precision by combining diagrammatic Monte Carlo and multi-histogram reweighting techniques. We observe that the mean field prediction in the continuous time limit captures the nonperturbative scaling, but receives a large, previously neglected correction on the unit prefactor. Using our nonperturbative prescription in place of the mean field result, we observe large corrections of the same magnitude to the continuous time limit of the static baryon mass, and of the location of the phase boundary associated with chiral symmetry restoration. In particular, the phase boundary, evaluated on different finite lattices, has a dramatically smaller dependence on the lattice time extent. We also estimate, as a byproduct, the pion decay constant and the chiral condensate of massless  $SU(3)$  QCD in the strong coupling limit at zero temperature.

---

<sup>\*</sup>forcrand@phys.ethz.ch

<sup>†</sup>wunger@physik.uni-bielefeld.de

<sup>‡</sup>helvio.vairinhos@gmail.com

# 1 Introduction

For all practical purposes, the sign problem in lattice QCD with staggered fermions at finite density has been solved at strong coupling. By integrating out the gauge degrees of freedom exactly – which allows replacing Grassmann integration by a sum over fermionic color singlets – the sign problem becomes mild enough to allow for controlled numerical results at moderate volumes, by combining importance sampling and reweighting methods. As a result, the phase diagram of lattice QCD in the strong coupling limit [1] and at first order in the strong coupling expansion [2] can be completely mapped.

In practice, however, it is not sufficient to simulate the strongly-coupled theory directly on rectangular lattices, because the critical temperature of chiral symmetry restoration is higher than what can be reached using the smallest lattice time extent.<sup>1</sup> In order to study the thermodynamical properties of staggered lattice QCD, in particular across the chiral phase transition, it is therefore necessary to simulate the theory on anisotropic lattices.

On anisotropic lattices, one assigns independent lattice spacings to the spatial and temporal directions, respectively  $a$  and  $a_t$ . The corresponding physical extents of the lattice can then be varied continuously, and independently. A more useful parameterisation of the lattice geometry uses the spatial lattice spacing,  $a$ , and the anisotropy parameter  $\xi$ ,

$$\xi = \frac{a}{a_t} \quad (1.1)$$

which becomes unity when the lattice is isotropic, and diverges in the continuous time limit. In this parameterisation, the lattice temperature is given by:

$$aT = \frac{\xi}{N_t} \quad (1.2)$$

where  $N_t$  is the lattice time extent. Hence, the lattice temperature can be varied continuously, through  $\xi$ .

In lattice gauge theory, the physical parameters  $a$  and  $\xi$  can only be varied implicitly, through independent bare parameters: the bare gauge coupling  $\beta$  and the bare anisotropy coupling  $\gamma$ . These bare parameters couple differently to the spatial and temporal plaquettes in the Wilson action of  $SU(N_c)$  or  $U(N_c)$  pure lattice gauge theory in  $d + 1$  dimensions [3]:

$$S_g = \frac{\beta}{\gamma} \sum_x \sum_{1 \leq i < j \leq d} \left( 1 - \frac{1}{N_c} \text{ReTr} (U_{x,ij}) \right) + \beta \gamma \sum_x \sum_{i=1}^d \left( 1 - \frac{1}{N_c} \text{ReTr} (U_{x,i0}) \right) \quad (1.3)$$

where  $U_{x,\mu\nu}$  is the ordered product of link variables around a plaquette parallel to the  $\hat{\mu}$  and  $\hat{\nu}$  directions.

For a single flavour of staggered fermions in the strong coupling limit ( $\beta = 0$ ), the anisotropic lattice action is given by:

$$S_f = 2a_t m_q \sum_x \bar{\psi}_x \psi_x + \sum_x \sum_{\mu=0}^d \gamma^{\delta_{\mu 0}} \eta_{x\mu} \left( e^{a_t \mu_q \delta_{\mu 0}} \bar{\psi}_x U_{x\mu} \psi_{x+\hat{\mu}} - e^{-a_t \mu_q \delta_{\mu 0}} \bar{\psi}_{x+\hat{\mu}} U_{x\mu}^\dagger \psi_x \right) \quad (1.4)$$

where  $a_t m_q$  and  $a_t \mu_q$  are the bare quark mass and quark chemical potential, respectively, and  $\eta_{x\mu} = \pm 1$  are the staggered phases. In the case of  $U(N_c)$ , gauge invariance dictates that color singlets are independent of  $a_t \mu_q$ , hence we may set  $a_t \mu_q$  to zero without loss of generality.

How  $a$  and  $\xi$  depend on the bare parameters of the theory is unknown a priori. This knowledge is, however, essential for precision measurements on anisotropic lattices, *e.g.* bulk thermodynamic quantities, and any uncontrolled approximation can easily be the main source of systematic errors.

In the weak gauge coupling regime ( $\beta \rightarrow \infty$ ) of the  $SU(N_c)$  pure gauge theory Eq. (1.3), perturbation theory and the non-renormalisation of the speed of light can be used to calibrate the anisotropy coupling [4]. In that regime, it is found that  $\xi_{\text{pert}}(\gamma) = \gamma$  (as expected classically).

<sup>1</sup> With staggered fermions, the spacetime lattice is necessarily bipartite. In particular, on a rectangular lattice it has an even number of lattice points in each direction. In this case, the lattice time extent is  $N_t \geq 2$ , hence the lattice temperature is  $aT = \frac{1}{N_t} \leq 0.5 < aT_c$ .

Using mean field techniques, the behaviour of the renormalised anisotropy at strong coupling ( $\beta \ll 1$ ) and at large values of  $\gamma$  is predicted to be quadratic, with unit prefactor [5]:

$$\xi_{\text{mf}}(\gamma) = \gamma^2 \quad (1.5)$$

In the nonperturbative regime, however, the relation between bare and renormalised anisotropy couplings can only be determined numerically. This has been done, for example, in pure gauge theory [3,6], or in lattice QCD with staggered fermions [7]. The nonperturbative renormalisation of the bare parameters requires fine-tuning, guided by some physical criterion which controls the recovery of Euclidean symmetry.

In this Letter we present a simple, precise, and nonperturbative method to calibrate the anisotropy coupling in lattice QCD with massless staggered fermions, in the limit of strong gauge coupling.

## 2 Diagrammatic representation of lattice QCD

The partition function of  $SU(N_c)$  or  $U(N_c)$  QCD on a bipartite  $N_t \times N_s^d$  lattice, with a single flavor of staggered fermions, in the strong coupling limit ( $\beta \rightarrow 0$ ), is given by:

$$Z = \int \mathcal{D}U \mathcal{D}\psi \mathcal{D}\bar{\psi} e^{2a_t m_q \sum_x \bar{\psi}_x \psi_x + \sum_{x,\mu} \gamma^{\delta\mu 0} \eta_{x\mu} (e^{a_t \mu q \delta\mu 0} \bar{\psi}_x U_{x\mu} \psi_{x+\hat{\mu}} - e^{-a_t \mu q \delta\mu 0} \bar{\psi}_{x+\hat{\mu}} U_{x\mu}^\dagger \psi_x)} \quad (2.1)$$

It factorises into a product of solvable fermionic one-link integrals.

In the  $SU(N_c)$  case, the group integration of the link variables, followed by the Grassmann integration of the fermionic degrees of freedom, yields the partition function of a monomer-dimer-loop model [8]:

$$Z = \sum_{\{n, k, \ell\}} \left( \prod_x \frac{N_c!}{n_x!} \right) \left( \prod_{x,\mu} \frac{(N_c - k_{x\mu})!}{N_c! k_{x\mu}!} \right) \frac{\sigma(\ell)}{N_c! |\ell|} (2a_t m_q)^{N_M} \gamma^{2N_{Dt} + N_c N_{\ell t}} e^{N_c N_t a_t \mu_q w(\ell)} \quad (2.2)$$

This partition function is a constrained sum over integer occupation numbers of monomers and dimers,  $n_x, k_{x\mu} \in \{0, 1, \dots, N_c\}$ , and of oriented baryon links,  $\ell_{x\mu} \in \{0, \pm 1\}$ , which combine to form oriented baryon loops. The global quantities:

$$N_M = \sum_x n_x, \quad N_{Dt} = \sum_x k_{x0}, \quad N_{\ell t} = \sum_x |\ell_{x0}| \quad (2.3)$$

enumerate the monomers, temporal dimers, and temporal baryon links on the lattice, respectively.  $\sigma(\ell) = \pm 1$  is a geometric sign associated with the configuration of baryon loops  $\ell$ ,  $|\ell|$  is their length, and  $w(\ell)$  is their winding number around the Euclidean time direction.

The monomers represent fermion condensates,  $M_x^{n_x}$ , dimers represent meson hoppings,  $(M_x M_{x+\hat{\mu}})^{k_{x\mu}}$ , and baryon links represent baryon hoppings,  $\bar{B}_x B_{x+\hat{\mu}}$  or  $\bar{B}_{x+\hat{\mu}} B_x$ , where  $M_x$  is a meson and  $B_x$  is a baryon:

$$M_x = \bar{\psi}_x \psi_x \quad (2.4a)$$

$$B_x = \frac{1}{N_c!} \varepsilon_{i_1 \dots i_{N_c}} \psi_x^{i_1} \dots \psi_x^{i_{N_c}} \quad (2.4b)$$

In order for a configuration of occupation numbers to contribute non-trivially to the partition function Eq. (2.2), the Grassmann integrals over the corresponding fermionic degrees of freedom must be non-trivial on each lattice site.

Due to their Grassmann nature, such configurations must necessarily represent arrangements of exactly  $N_c$  fermions and  $N_c$  anti-fermions on each lattice site.<sup>2</sup> This imposes the following local constraints on the integer occupation numbers:

$$n_x + \sum_{\pm\mu} \left( k_{x\mu} + \frac{N_c}{2} |\ell_{x\mu}| \right) \stackrel{!}{=} N_c \quad (2.5a)$$

<sup>2</sup> If the gauge group is  $SU(N_c)$ , the ordering of the Grassmann variables in such arrangements contributes with the geometric sign  $\sigma(\ell) = \pm 1$ , which introduces a (baryonic) sign problem in the system. See Eq. (2.2).

$$\sum_{\pm\mu} \ell_{x\mu} \stackrel{!}{=} 0 \quad (2.5b)$$

Eq. (2.5b) is a local discrete conservation law for baryon links, which formalises our statement above that baryon links in admissible configurations form closed oriented loops.

In the  $U(N_c)$  case, since  $\ell_{x\mu} = 0$ , the partition function Eq. (2.2) reduces to a sum over monomer-dimer configurations:

$$Z = \sum_{\{n,k\}} \left( \prod_x \frac{N_c!}{n_x!} \right) \left( \prod_{x,\mu} \frac{(N_c - k_{x\mu})!}{N_c! k_{x\mu}!} \right) (2a_t m_q)^{N_M} \gamma^{2N_{D_t}} \quad (2.6)$$

with the same Grassmann constraint for monomers and dimers on each site:

$$n_x + \sum_{\pm\mu} k_{x\mu} \stackrel{!}{=} N_c \quad (2.7)$$

Likewise, the  $U(N_c)$  observables are defined in the same way as the observables (in the mesonic sector) of the  $SU(N_c)$  theory.

### 3 Conserved currents and conserved charges

Let  $\sigma_x = \pm 1$  be the parity of the site  $x$  on a bipartite lattice. From Eq. (2.5b), it is easy to construct baryonic currents:

$$j_{x\mu}^B = \sigma_x \ell_{x\mu} \quad (3.1)$$

which are conserved at every site:

$$\sum_{\mu=0}^d (j_{x\mu}^B - j_{x-\hat{\mu},\mu}^B) = 0 \quad (3.2)$$

The corresponding conserved charges are integrals of the baryonic currents Eq. (3.1) over a codimension-1 lattice slice  $\mathcal{S}_\mu$ , perpendicular to  $\hat{\mu}$ :

$$Q_\mu^B = \sum_{x \in \mathcal{S}_\mu} j_{x\mu}^B \quad (3.3)$$

Similarly, by rewriting Eq. (2.5a) as:

$$\sum_{\pm\mu} \left( k_{x\mu} + \frac{N_c}{2} |\ell_{x\mu}| - \frac{N_c}{2d} \right) = -n_x \quad (3.4)$$

it is easy to construct the corresponding (pion) currents:

$$j_{x\mu} = \sigma_x \left( k_{x\mu} + \frac{N_c}{2} |\ell_{x\mu}| - \frac{N_c}{2d} \right) \quad (3.5)$$

from which a local discrete Gauss' law for dimers results:

$$\sum_{\mu=0}^d (j_{x\mu} - j_{x-\hat{\mu},\mu}) = -\sigma_x n_x \quad (3.6)$$

Thus, monomers are sources of the pion currents. Using Grassmann variables, the source term on the r.h.s. of Eq. (3.6) corresponds to  $-a_t m_q \bar{\psi}_x \gamma_5 \psi_x$ . Only in the chiral limit, *i.e.* in the absence of monomers, are

the pion currents conserved. In the chiral limit, the corresponding conserved charges are integrals of the pion currents over a lattice slice  $\mathcal{S}_\mu$ :

$$Q_\mu = \sum_{x \in \mathcal{S}_\mu} j_{x\mu} \quad (3.7)$$

In the  $U(N_c)$  theory, since  $\ell_{x\mu} = 0$ , the pion currents simplify to:

$$j_{x\mu} = \sigma_x \left( k_{x\mu} - \frac{N_c}{2d} \right) \quad (3.8)$$

## 4 Nonperturbative anisotropy calibration

In this Section, we show how the conserved pion charges can be used to calibrate the anisotropy coupling in lattice QCD with staggered fermions, at zero temperature, in the strong coupling limit.

In the strong coupling limit, the partition functions of  $SU(N_c)$  and  $U(N_c)$  lattice QCD with staggered fermions have monomer-dimer-loop representations, Eqs. (2.2) and (2.6), with no dependence on the spatial lattice spacing,  $a$ . In order for the pion charges  $Q_\mu$  to be conserved, we take the lattice fermions to be massless,  $a_t m_q = 0$ . In the  $SU(N_c)$  case, we only consider the case of zero chemical potential,  $a_t \mu_q = 0$ .<sup>3</sup> The corresponding partition functions thus depend only on a single parameter: the bare anisotropy coupling  $\gamma$ .

Let us consider the theories to be defined on anisotropic  $N_t \times N_s^d$  lattices. In order to calibrate the anisotropy, we compare the fluctuations of the conserved pion charges in different directions.

Due to spatial isotropy, the expectation values of fluctuations of the spatial pion charges  $Q_i$ ,  $i = 1, \dots, d$  must coincide. Therefore, it is convenient to quantify spatial fluctuations using the expectation value of:

$$Q_s^2 = \frac{1}{d} \sum_{i=1}^d Q_i^2 \quad (4.1)$$

while the temporal fluctuations are quantified using the expectation value of  $Q_t^2 = Q_0^2$ .

Now, when the lattice is hypercubic, *i.e.*  $N_t = \xi N_s$ , the fluctuations of the spatial and temporal conserved charges must be equal. This provides a simple, nonperturbative criterion for the renormalisation of the anisotropy coupling: the value of the bare parameter,  $\gamma_{\text{np}}$ , corresponding to the renormalised value,  $\xi(\gamma_{\text{np}}) = N_t/N_s$ , is that for which the fluctuations of the spatial and temporal conserved charges are equal:

$$\langle Q_t^2 \rangle_{\gamma_{\text{np}}} \stackrel{!}{=} \langle Q_s^2 \rangle_{\gamma_{\text{np}}} \quad (4.2)$$

In Fig. 1, we give a practical example. In a numerical simulation of  $U(3)$  lattice QCD on a  $32 \times 16^3$  lattice, we evaluate  $\langle Q_s^2 \rangle$  and  $\langle Q_t^2 \rangle$  for a few values of the bare parameter  $\gamma$ , about the correct nonperturbative value  $\gamma_{\text{np}}$  associated with the renormalised anisotropy parameter,  $\xi = 2$ . Using Ferrenberg-Swendsen multi-histogram reweighting, we interpolate the measurements of the fluctuations, and estimate with high precision the value of the bare parameter for which the two curves intersect, *i.e.* when the lattice is hypercubic. In this particular case,  $\gamma_{\text{np}} = 1.55725(29)$  (see Table 1). This value is to be compared with the commonly accepted mean field prediction,  $\gamma_{\text{mf}} = \sqrt{\xi} = 2 \approx 1.41421$ .

## 5 Running anisotropy

It is also possible to estimate the running of the anisotropy parameter,  $\frac{1}{\xi} \frac{d\xi}{d\gamma}$ , using extra information from the intersection point in Fig. 1. This quantity – the strong-coupling analogue of Karsch’s coefficients [4] – is important for computing *e.g.* bulk thermodynamic quantities, like the energy density and pressure [10].

---

<sup>3</sup> The chemical potential only modifies the temporal boundary conditions, which is irrelevant at  $T = 0$ .

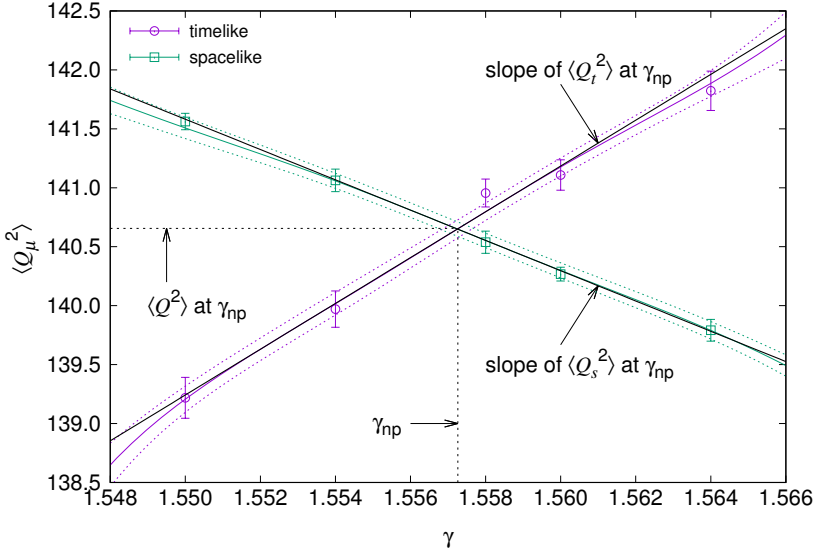


**Figure 1:** Measurements of the fluctuations of the conserved pion charges in a numerical simulation of U(3) lattice QCD on a  $32 \times 16^3$  lattice. The measurements are interpolated using Ferrenberg-Swendsen multi-histogram reweighting. The intersection of the two curves provides a precise nonperturbative estimate of the bare parameter  $\gamma_{np}$  associated with the renormalised anisotropy:  $\xi = 2$ . It also provides an estimate of the value of such fluctuations in the hypercubic lattice,  $\langle Q^2 \rangle$ , which, together with the estimates of the slopes of the tangents to the curves at the intersection point, allows an estimation of the running anisotropy,  $\frac{1}{\xi} \frac{d\xi}{d\gamma}$ .

The fluctuations of the conserved charges scale with the volume of the lattice slices on which the corresponding conserved currents are integrated over:

$$\langle Q_t^2 \rangle \propto (N_s a)^3 \quad (5.1a)$$

$$\langle Q_s^2 \rangle \propto (N_s a)^2 N_t a t \quad (5.1b)$$

The ratio of temporal and spatial fluctuations then becomes directly related to the renormalised anisotropy:

$$\frac{\langle Q_t^2 \rangle}{\langle Q_s^2 \rangle} = \frac{N_s}{N_t} \xi \quad (5.2)$$

We have already explained the fact that this ratio is 1 when the lattice is hypercubic.

Now, taking the derivative of Eq. (5.2) with respect to the bare parameter  $\gamma$ , at the intersection of the curves in Fig. 1, yields the value of the running anisotropy at that point:

$$\frac{d}{d\gamma} \frac{\langle Q_t^2 \rangle}{\langle Q_s^2 \rangle} \Big|_{\gamma_{np}} = \frac{\langle Q_t^2 \rangle'_{\gamma_{np}} - \langle Q_s^2 \rangle'_{\gamma_{np}}}{\langle Q^2 \rangle_{\gamma_{np}}} = \frac{N_s}{N_t} \frac{d\xi}{d\gamma} \Big|_{\gamma_{np}} = \frac{1}{\xi} \frac{d\xi}{d\gamma} \Big|_{\gamma_{np}} \quad (5.3)$$

Therefore, in order to estimate the value of the running anisotropy at  $\gamma_{np}$ , we also need the value of the fluctuation of the conserved pion charges on a hypercubic lattice:

$$\langle Q^2 \rangle_{\gamma_{np}} \equiv \langle Q_t^2 \rangle_{\gamma_{np}} \stackrel{!}{=} \langle Q_s^2 \rangle_{\gamma_{np}} \quad (5.4)$$

and the values of the slopes of the tangents to the curves at the intersection point:  $\langle Q_t^2 \rangle'_{\gamma_{np}}$  and  $\langle Q_s^2 \rangle'_{\gamma_{np}}$ .

## 6 Numerical renormalisation

The Monte Carlo sampling of the  $U(N_c)$  partition function Eq. (2.6) is highly efficient when using directed path algorithms [9]. In the  $SU(N_c)$  case, observables must be reweighted because of the occurrence of negative baryonic configurations, even at zero chemical potential. However, this sign problem is mild and controllable for moderate lattice volumes [1,2,10].

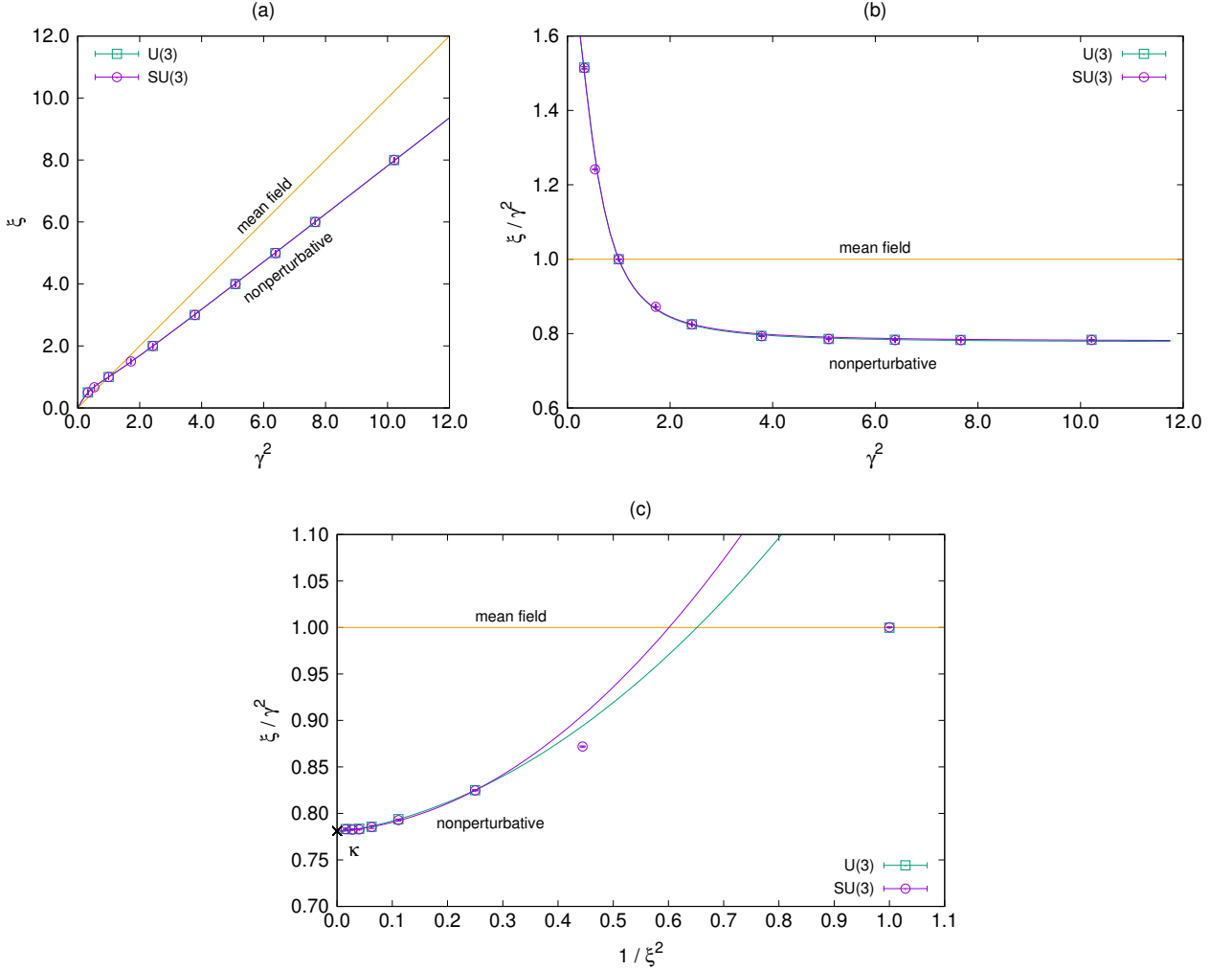


**Figure 2:** Nonperturbative relation between the bare and renormalised anisotropy parameters, for U(3) (green) and SU(3) (purple) lattice QCD, in the thermodynamic limit, presented in 3 different ways. Fig. 2a shows that, as predicted by mean-field, the renormalised anisotropy at large  $\gamma$  is  $\xi(\gamma) \propto \gamma^2$ , but with a smaller prefactor than predicted. Fig. 2b shows the ratio  $\xi/\gamma^2$  for a wide range of  $\gamma$ , larger and smaller than 1. A simple one-parameter Ansatz Eq. (6.2) describes the data well. Fig. 2c shows the approach to the continuous time limit, i.e.  $\xi \rightarrow \infty$ . In that regime,  $\xi/\gamma^2$  approaches a constant  $\kappa$ , with quadratic corrections in  $1/\xi^2$ . The behaviours of U(3) and SU(3) are almost undistinguishable, because baryons are heavy and describe small loops only.

We simulate massless U(3) and SU(3) lattice QCD in the strong coupling limit, using the directed path algorithm [9], for several values of the renormalised anisotropy  $\xi$ . For each  $\xi$ , we estimate the corresponding value of the bare parameter  $\gamma_{np}$  on a  $(\xi N_s) \times N_s^3$  lattice, for several values of  $N_s$ , using the method described in Section 4. We also measure the running of the anisotropy coupling Eq. (5.3). The results are summarised in Tables 1 and 2.

In these tables, rather than storing the estimators of Eq. (5.3), we instead store the estimators of its reciprocal, the reason being that the latter enters linearly in the definition of important bulk thermodynamic quantities, *e.g.* the energy density:

$$a^4 \epsilon = \frac{a^4}{V} \frac{\partial \log Z}{\partial T^{-1}} = \frac{\xi}{\gamma} \frac{d\gamma}{d\xi} \frac{2\xi \langle N_{Dt} \rangle}{N_s} \quad (6.1)$$

The nonperturbative relation between the renormalised and bare anisotropy parameters, in the thermodynamic limit, is presented in Fig. 2a. At large anisotropies, the renormalised parameter depends quadratically on the bare parameter. Such a behaviour is expected from mean field arguments. However, the cor-

responding prefactor differs significantly ( $\approx 25\%$ ) from that of the mean field relation Eq. (1.5). This introduces a significant systematic error in any numerical study of strongly-coupled lattice QCD.

We find that the whole range of measurements is well described by a simple, one-parameter rational Ansatz (see Fig. 2b):

$$\frac{\xi(\gamma)}{\gamma^2} \approx \kappa + \frac{1}{1 + \lambda\gamma^4} \quad (6.2)$$

where  $\kappa$  is a constant, and  $\lambda \stackrel{!}{=} \kappa/(1 - \kappa)$ , from the requirement that  $\xi(1) \stackrel{!}{=} 1$ . The approach to the continuous time limit is better captured by Taylor expanding Eq. (6.2) to quadratic order in  $1/\xi^2$  (see Fig. 2c):

$$\frac{\xi(\gamma)}{\gamma^2} \approx \kappa \left( 1 + \frac{c_1}{\xi^2} + \frac{c_2}{\xi^4} \right) \quad (6.3)$$

The fitted values of  $\kappa$  using the Ansatz Eq. (6.3) – consistent with those obtained using the Ansatz Eq. (6.2) – are:

$$\kappa = \begin{cases} 0.7795(4), & \text{U(3)} \\ 0.7810(8), & \text{SU(3)} \end{cases} \quad (6.4)$$

where errors are statistical only. This prefactor is significantly different from the mean field value 1.

Values for U(3) and SU(3) are statistically consistent with each other. This is to be expected: in the continuous time limit, baryons become increasingly static, and their effect on pion currents vanishes at  $T = 0$ .

The Ansatz Eq. (6.2) is also consistent, after differentiation, with the Monte Carlo data for the running anisotropy. In particular, for the isotropic case, instead of the mean field value:

$$\frac{1}{\xi_{\text{mf}}} \frac{d\xi_{\text{mf}}}{d\gamma} \Big|_{\gamma=1} = 2 \quad (6.5)$$

we find nonperturbative corrections consistent with:

$$\frac{1}{\xi} \frac{d\xi}{d\gamma} \Big|_{\gamma=1} \approx 2 + 4\kappa(\kappa - 1) \quad (6.6)$$

## 7 Applications

In this Section, we use the nonperturbative relation between  $\xi$  and  $\gamma$ , determined above, in order to control the convergence of several physical quantities to their continuous time limits.

First, we examine the  $N_t$ -dependence of the phase boundary of the  $(\mu_q, T)$  phase diagram of massless SU(3) lattice QCD, and its sensitivity to the anisotropy prescription. Then, we estimate the continuous time values of the static baryon mass  $am_B$ , the pion decay constant  $aF_\pi$ , and the infinite-volume chiral condensate  $a^3\Sigma$ , in massless U(3) or SU(3) lattice QCD. We use a quadratic Ansatz in  $1/\xi^2$  to model the anisotropy corrections to the continuous time limit:

$$\mathcal{O} \approx \mathcal{O}^{\text{CT}} \left( 1 + \frac{c_1}{\xi^2} + \frac{c_2}{\xi^4} \right) \quad (7.1)$$

where  $\mathcal{O}$  is one of the physical quantities listed above, and  $\mathcal{O}^{\text{CT}}$  is the corresponding continuous time value.

For the computation of the pion decay constant and of the chiral condensate, we use the fact that U(3) and SU(3) lattice QCD with massless staggered fermions have an exact  $O(2)$  chiral symmetry. At  $T = 0$  this symmetry is spontaneously broken, and the dynamics of the resulting Goldstone degrees of freedom (pions) are well described by an  $O(2)$  sigma model in  $d = 4$  dimensions. From a finite-size scaling analysis of the discrete  $O(2)$  model, it is then possible to extract low-energy quantities like  $F_\pi$  and  $\Sigma$ .

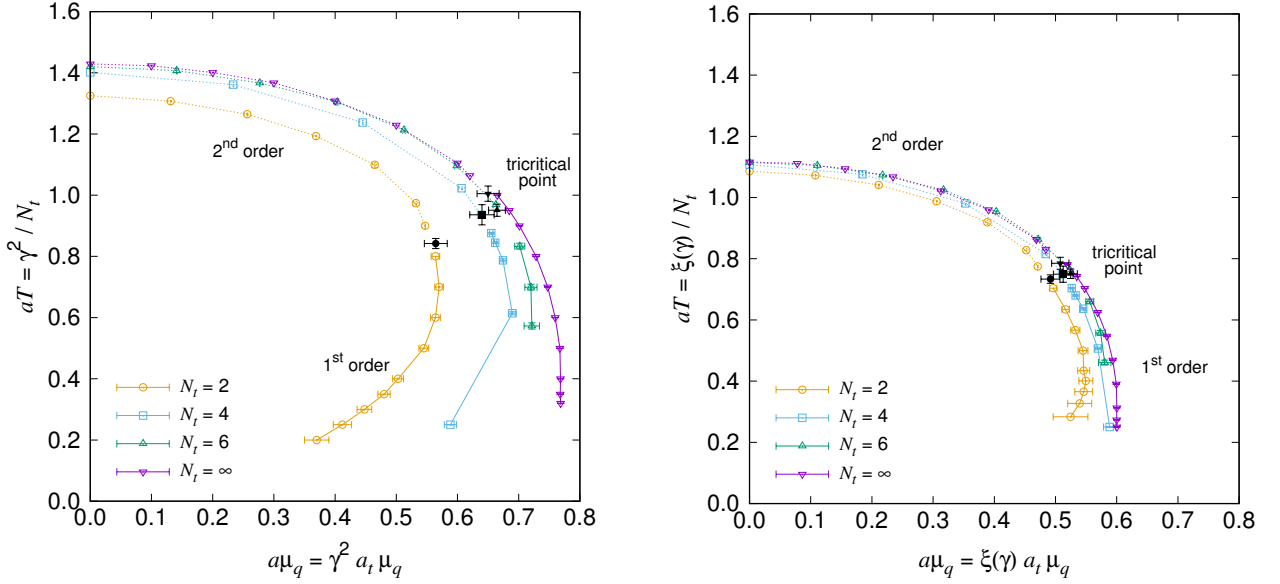


**Figure 3:** Phase diagram of  $SU(3)$  lattice QCD with massless staggered fermions, in the strong coupling limit, in which the anisotropy is set using mean field (left) [2], or using the present nonperturbative prescription (right). Under the nonperturbative prescription Eq. (6.2), the  $N_t$ -dependence of the phase boundary and of the tricritical point decreases substantially. Also, the tricritical couplings on the horizontal and vertical axes both decrease by  $\approx 25\%$ . The  $N_t = \infty$  data is produced from simulations directly in the continuous time limit [13].

For example, the pion decay constant at  $T = 0$  can be shown to be related to the helicity modulus  $Y$  [12]:

$$a^2 F_\pi^2 = \lim_{N_s \rightarrow \infty} a^2 Y \quad (7.2)$$

which corresponds, in the diagrammatic representation, to the variance of the conserved pion charges  $Q_\mu$  on a hypercubic lattice [11]:

$$a^2 Y = \frac{1}{N_s^2} \langle Q^2 \rangle_{\gamma_{\text{np}}} \quad (7.3)$$

In turn, the chiral condensate at  $T = 0$  can be estimated from the finite-size scaling of the chiral susceptibility  $\chi$ , evaluated on hypercubic lattices. This has been done in  $d = 3 + 1$  at finite temperature [11]. Chiral perturbation theory of the  $O(2)$  model predicts the leading finite-size corrections to be of the form [12]:

$$a^6 \chi \approx \frac{1}{2} a^6 \Sigma^2 N_s^4 \left( 1 + \frac{\beta_1}{a^2 F_\pi^2 N_s^2} + \frac{1}{2a^4 F_\pi^4 N_s^4} \left( \beta_1^2 + \beta_2 + \frac{1}{8\pi^2} \log \frac{a \Lambda_\Sigma^2 N_s}{\Lambda_M} \right) \right) \quad (7.4)$$

where  $\beta_1 = 0.140461$ ,  $\beta_2 = -0.020305$ , and  $\Lambda_\Sigma, \Lambda_M$  are renormalisation group invariant scales. The average value of the chiral susceptibility is estimated using intermediate configurations – generated with the directed path algorithm – which sample the mesonic two-point function, as described in [9].

**Phase diagram** An example of a study that is sensitive to the choice of an anisotropy prescription is the mapping of the phase diagram of massless  $SU(3)$  lattice QCD, in the strong coupling limit [1].

The phase boundary separating the chirally broken phase at low  $(\mu_q, T)$  and the chirally symmetric phase at high  $(\mu_q, T)$  is determined by monitoring the chiral condensate  $a^3 \Sigma$  during Monte Carlo simulations, using directed path algorithms and sign reweighting for importance sampling on moderate volumes (see Fig. 3).

For fixed  $N_t$ , the temperature is varied implicitly through the bare coupling  $\gamma$  [2]. Assuming the mean field relation Eq. (1.5), the observed phase boundary has a strong dependence on  $N_t$  (see Fig. 3, left), which

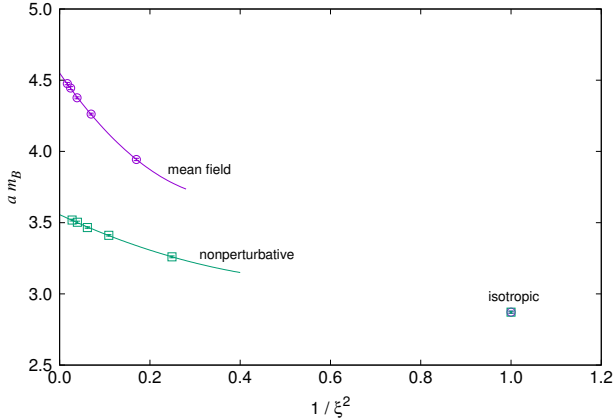


**Figure 4:** Effect of the physical anisotropy on the static baryon mass, in massless SU(3) lattice QCD. The anisotropy corrections to the continuous time limit ( $\xi \rightarrow \infty$ ) are well described by a quadratic Ansatz in  $1/\xi^2$ . The baryon mass is heavier on anisotropic lattices than on isotropic lattices, where its value is  $am_B \approx 2.88$  [1]. With the anisotropy set using mean field, the baryon mass receives an  $\approx 50\%$  correction in the continuous time limit with respect to the isotropic case, while under the present nonperturbative prescription it only receives an  $\approx 20\%$  correction.

makes its interpretation questionable. This systematic error is dramatically reduced by using the nonperturbative prescription Eq. (6.2) for the renormalised anisotropy (see Fig. 3, right). Note that, under the nonperturbative prescription, the tricritical couplings on the temperature and chemical potential axes both decrease by  $\approx 25\%$ .

Note that analytic studies of the phase diagram generally consider Euclidean time as continuous [14], and should be compared with the  $N_t = \infty$  data only.

**Static baryon mass** The static baryon mass  $am_B$  is another observable for which the inexact calibration of anisotropy can have a strong effect. This observable can be determined using the “snake algorithm” [15], which samples partition functions  $Z_k$  describing the system with an open baryonic segment of length  $k$ :

$$am_B = \frac{\xi}{N_t} \sum_{k=0}^{N_t-2} \log \frac{Z_{k+2}}{Z_k} \quad (7.5)$$

We simulate massless SU(3) lattice QCD for different anisotropies using the snake algorithm, and estimate  $am_B$  as a function of  $\xi$  (see Fig. 4 and Table 3). Under the two anisotropy prescriptions, Eqs. (1.5) and (6.2), baryon masses differ by  $\approx 25\%$  at large  $\xi$ . In this regime, the fitting Ansatz Eq. (7.1) describes the data well. The vertical intercepts give the values of the static baryon mass in the continuous time limit:

$$(am_B)^{\text{CT}} = \begin{cases} 4.550(8), & \text{mean field} \\ 3.556(6), & \text{nonperturbative} \end{cases} \quad (7.6)$$

On an isotropic lattice, static baryons have mass  $am_B \approx 2.88$  [1], and become heavier with anisotropy. In the continuous time limit, the baryon mass is only  $\approx 20\%$  heavier than the isotropic case, when using the nonperturbative prescription for the anisotropy, as compared with the  $\approx 50\%$  difference when using mean field.

**Pion decay constant** Using our nonperturbative prescription for  $\xi$ , we can obtain reliable estimates of several physical quantities in the continuous time limit, *e.g.* the pion decay constant,  $aF_\pi$ . In order to estimate this quantity, we measure the helicity modulus Eq. (7.3) for several finite hypercubic lattices and values of  $\xi$ . The results are summarised in Tables 1 and 2, and displayed in Fig. 5 (left). The pion decay constant (squared) corresponds to the thermodynamic limit of the helicity modulus, in accordance with Eq. (7.2).

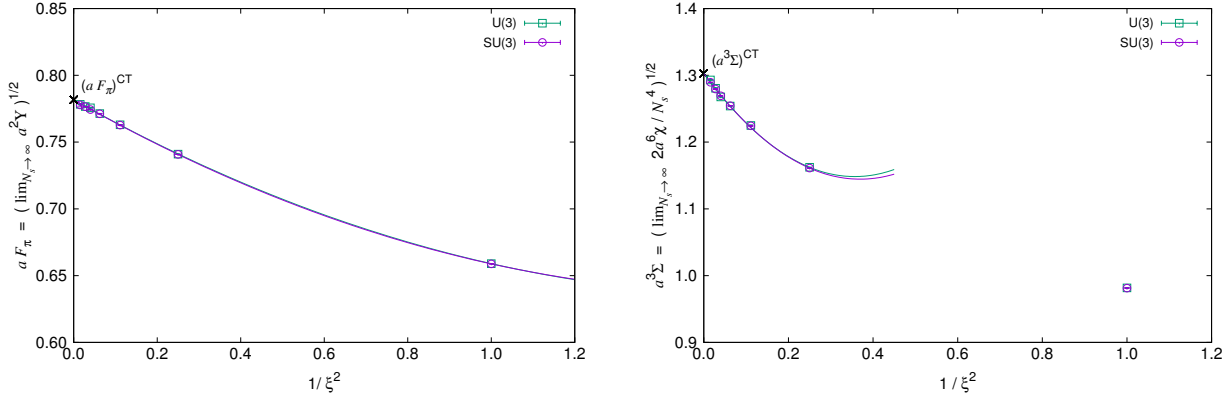


**Figure 5:** Effect of the physical anisotropy on the pion decay constant (left) and on the chiral condensate (right), in massless U(3) and SU(3) lattice QCD. The anisotropy corrections to the continuous time limit ( $\xi \rightarrow \infty$ ) are rather small, and well described by a quadratic Ansatz in  $1/\xi^2$ . The baryonic corrections to the U(3) helicity modulus are negligible.

Again, the numerical data can be suitably fitted using the Ansatz Eq. (7.1). At large  $\xi$ , the anisotropy corrections are rather small. The vertical intercepts give the values of the pion decay constant in the continuous time limit at  $T = 0$ :

$$(aF_\pi)^{\text{CT}} = \begin{cases} 0.7816(4), & \text{U(3)} \\ 0.7817(2), & \text{SU(3)} \end{cases} \quad (7.7)$$

Again, U(3) and SU(3) are equivalent in the thermodynamic and continuous time limits, within errors.

**Chiral condensate** We also estimate accurate values for the infinite-volume chiral condensate  $a^3\Sigma$ , by analysing the finite-size scaling of the chiral susceptibility  $a^6\chi$ , using chiral perturbation theory, and by using our nonperturbative prescription for the lattice anisotropy.

To this end, we estimate the chiral susceptibility density  $a^6\chi / N_s^4$  (as in [9]) for several finite hypercubic lattices and values of  $\xi$  (see Tables 1 and 2). We estimate  $a^6\Sigma^2$  at finite  $\xi$  by extrapolating  $a^6\chi / N_s^4$  to the thermodynamic limit, by modelling the finite-size corrections in accordance with chiral perturbation theory, see Eq. (7.4).

The dependence of  $a^3\Sigma$  on  $\xi$  is again well described by the Ansatz Eq. (7.1) (see Fig. 5, right). The vertical intercepts give the values of the chiral condensate in the continuous time limit at  $T = 0$ :

$$(a^3\Sigma)^{\text{CT}} = \begin{cases} 1.303(4), & \text{U(3)} \\ 1.3026(4), & \text{SU(3)} \end{cases} \quad (7.8)$$

As before, U(3) and SU(3) are equivalent in the thermodynamic and continuous time limits, within errors. We also observe that, when keeping  $\beta_1$  as a free parameter, the fits are consistent with its theoretical value.

## Conclusion

It is very important to have a precise scale for the lattice anisotropy. Even though mean field captures the correct power scaling of the renormalised anisotropy for asymptotically large values of the bare anisotropy, namely  $\xi \sim \gamma^2$ , it fails to predict the nonperturbative prefactor. The discrepancy between the mean field and nonperturbative prefactors introduces systematic errors of the same magnitude in many physical quantities of interest, particularly in the continuous time limit. This should be kept in mind when comparing strong-coupling Monte Carlo results and analytic mean field results, since the latter are usually formulated in continuous time.

In the dimer representation of the strong coupling limit of lattice QCD with massless staggered fermions, we have proposed a simple method to determine the nonperturbative dependence  $\xi(\gamma)$  between the bare

and renormalised anisotropy couplings. The method is amenable to Monte Carlo simulations using very efficient directed path algorithms which, together with the multi-histogram reweighting method, allows us to determine  $\xi(\gamma)$  with high precision. In the end, the nonperturbative prefactor is observed to be off by  $\approx 25\%$  with respect to the mean field prefactor.

As an application, we update the phase diagram of SU(3) lattice QCD [1], and compute the mass of a static baryon in the continuous time limit, using our nonperturbative relation  $\xi(\gamma)$ . On the phase diagram, a strong dependence of the phase boundaries on  $N_t$ , introduced by the mean field anisotropy, essentially vanishes. The values of the static baryon mass in the continuous time limit, and of the critical points on the temperature and chemical potential axes of the phase diagram, reveal corrections with respect to the mean field values of the same magnitude as the prefactor, *i.e.*  $\approx 25\%$ .

We also estimate the values of the pion decay constant,  $aF_\pi$ , and of the infinite-volume chiral condensate,  $a^3\Sigma$ , in massless lattice QCD in the strong coupling limit at  $T = 0$ . The anisotropy corrections to these quantities are small, and provide a reliable extrapolation to their continuous time limits.

Even though the strong coupling limit of lattice QCD is unphysical, it is still interesting to compare its predictions with those of continuum QCD, in the regime where chiral symmetry is spontaneously broken. For example, the strong-coupling SU(3) lattice value of the pion decay constant Eq. (7.7), in units of the critical temperature  $aT_c \approx 1.089$  [10], is  $F_\pi/T_c \approx 0.72$ , which is about 15% above the continuum QCD value.

The renormalisation criterion Eq. (4.2) relies on the conservation of the pion currents Eq. (3.5). At non-zero quark mass, however, the pion current is no longer conserved, as per Eq. (3.6). In order for a similar criterion to work for finite quark mass, the latter must also be renormalised. Such an extension of the present study seems possible, the only penalty being an increased numerical effort.

It may also be possible to extend the present study to finite  $\beta$ , in the framework of the  $O(\beta)$  partition function defined in [2]. The new occupation numbers (associated with plaquettes) introduce new Grassmann constraints on the extended configuration space. Such constraints may be used to construct analogues of the pion current, which would include plaquette corrections. In the chiral limit, we expect such currents to be conserved. The associated conserved charges could then be used to define nonperturbative renormalisation criteria for the (independent) spatial and temporal gauge couplings. An extension of this program to finite quark mass would be similar to the above proposal for  $\beta = 0$ .

## Acknowledgements

We are very grateful to Oscar Åkerlund, Tobias Rindlisbacher, and Paul Romatschke for many useful discussions. We are also grateful to the Mainz Institute for Theoretical Physics (MITP) for its hospitality and its partial support during the completion of this work. Numerical simulations were performed on the Brutus and Euler clusters at ETH Zürich, and on the OCULUS cluster at PC<sup>2</sup> (Universität Paderborn). This work is supported by the Swiss National Science Foundation under the grant 200020\_162515. WU is supported by the Emmy Noether Program under the grant UN 370/1-1.

## References

- [1] P. de Forcrand and M. Fromm, Phys. Rev. Lett. **104** (2010) 112005 [[url](#)] [[arXiv:0907.1915](#)] [hep-lat].
- [2] P. de Forcrand, J. Langelage, O. Philipsen and W. Unger, Phys. Rev. Lett. **113** (2014) 152002 [[url](#)] [[arXiv:1406.4397](#)] [hep-lat].
- [3] J. Engels, F. Karsch, H. Satz and I. Montvay, Nucl. Phys. B **205** (1982) 545 [[url](#)]. G. Burgers, F. Karsch, A. Nakamura and I. O. Stamatescu, Nucl. Phys. B **304** (1988) 587 [[url](#)];
- [4] F. Karsch, Nucl. Phys. B **205** (1982) 285 [[url](#)]; F. Karsch and I. O. Stamatescu, Phys. Lett. B **227** (1989) 153 [[url](#)].
- [5] G. Faldt and B. Petersson, Nucl. Phys. B **265** (1986) 197 [[url](#)]; N. Bilic, F. Karsch and K. Redlich, Phys. Rev. D**45** (1992) 3228 [[url](#)].

- [6] G. Boyd, J. Engels, F. Karsch, E. Laermann, C. Legeland, M. Lutgemeier and B. Petersson, Nucl. Phys. B **469** (1996) 419 [[url](#)] [[hep-lat/9602007](#)]; F. Karsch, J. Engels and T. Scheideler, Nucl. Phys. Proc. Suppl. **63** (1998) 427 [[url](#)] [[hep-lat/9709011](#)]; T. R. Klassen, Nucl. Phys. B **533** (1998) 557 [[url](#)] [[hep-lat/9803010](#)]; S. Ejiri, Y. Iwasaki and K. Kanaya, Phys. Rev. D **58** (1998) 094505 [[url](#)] [[hep-lat/9806007](#)]; J. Engels, F. Karsch and T. Scheideler, Nucl. Phys. B **564** (2000) 303 [[url](#)] [[hep-lat/9905002](#)].
- [7] L. Levkova and T. Manke, Nucl. Phys. Proc. Suppl. **106** (2002) 218 [[url](#)] [[hep-lat/0110171](#)]; L. Levkova, Nucl. Phys. Proc. Suppl. **119** (2003) 520 [[url](#)] [[hep-lat/0209069](#)]; K. Nomura, T. Umeda and H. Matsufuru, Nucl. Phys. Proc. Suppl. **129** (2004) 390 [[url](#)] [[hep-lat/0312010](#)]; K. Nomura, H. Matsufuru and T. Umeda, Prog. Theor. Phys. **111** (2004) 245 [[url](#)] [[hep-lat/0401009](#)].
- [8] P. Rossi and U. Wolff, Nucl. Phys. B **248** (1984) 105 [[url](#)]; F. Karsch and K. H. Mutter, Nucl. Phys. B **313** (1989) 541 [[url](#)].
- [9] D. H. Adams and S. Chandrasekharan, Nucl. Phys. B **662** (2003) 220 [[url](#)] [[hep-lat/0303003](#)].
- [10] P. de Forcrand, P. Romatschke, W. Unger and H. Vairinhos, PoS LATTICE **2016** (2017) 086 [[arXiv:1701.08324](#)] [[hep-lat](#)].
- [11] S. Chandrasekharan and F. J. Jiang, Phys. Rev. D **68** (2003) 091501 [[url](#)] [[hep-lat/0309025](#)].
- [12] P. Hasenfratz and H. Leutwyler, Nucl. Phys. B **343** (1990) 241 [[url](#)]
- [13] W. Unger and P. de Forcrand, PoS LATTICE **2011** (2011) 218 [[arXiv:1111.1434](#)] [[hep-lat](#)].
- [14] P. H. Damgaard, N. Kawamoto and K. Shigemoto, Phys. Rev. Lett. **53** (1984) 2211 [[url](#)]; P. H. Damgaard, D. Hochberg and N. Kawamoto, Phys. Lett. **158B** (1985) 239 [[url](#)]; P. H. Damgaard, N. Kawamoto and K. Shigemoto, Nucl. Phys. B **264** (1986) 1 [[url](#)]; Y. Nishida, Phys. Rev. D **69** (2004) 094501 [[url](#)] [[hep-ph/0312371](#)].
- [15] P. de Forcrand, M. D'Elia and M. Pepe, Phys. Rev. Lett. **86** (2001) 1438 [[url](#)] [[hep-lat/0007034](#)].

$\xi$	$N_s$	$\gamma_{\text{np}}$	$\frac{\xi}{\gamma} \frac{d\gamma}{d\xi} \Big _{\gamma_{\text{np}}}$	$a^2 Y$	$N_s^{-4} a^6 \chi$
1/2	8	0.5741(2)	0.436(9)	0.27470(8)	0.283790(5)
	12	0.5745(2)	0.453(8)	0.27491(2)	0.282627(8)
	16	0.5743(2)	0.43(1)	0.274790(8)	0.282207(4)
	20	0.5743(4)	0.44(2)	0.27480(2)	0.282091(4)
	24	0.5744(5)	0.45(3)	0.27470(2)	0.282154(7)
1	4	1.00000(5)	0.357(2)	0.433247(7)	0.489464(1)
	6	1.0000(5)	0.39(2)	0.43386(2)	0.485833(9)
	8	0.9998(4)	0.35(2)	0.43406(2)	0.484282(7)
	10	1.0000(5)	0.36(3)	0.43419(2)	0.483401(6)
2	4	1.55748(8)	0.284(2)	0.548976(1)	0.683808(2)
	6	1.5570(4)	0.28(2)	0.54933(2)	0.67935(2)
	8	1.557(2)	0.37(5)	0.54945(3)	0.67775(2)
	10	1.5565(9)	0.27(4)	0.54889(3)	0.67696(2)
	12	1.5566(8)	0.26(3)	0.54914(4)	0.67636(2)
3	4	1.9447(2)	0.260(4)	0.582237(6)	0.761082(2)
	6	1.9431(8)	0.31(2)	0.58265(3)	0.75676(2)
	8	1.9446(7)	0.23(3)	0.58248(2)	0.75377(2)
	10	1.9443(9)	0.25(2)	0.58207(4)	0.75307(2)
4	4	2.2577(8)	0.27(2)	0.5949(2)	0.79818(1)
	6	2.2560(8)	0.26(3)	0.59548(2)	0.79385(2)
	8	2.2577(2)	0.27(2)	0.59531(2)	0.79074(2)
	10	2.2579(2)	0.30(3)	0.59505(4)	0.78932(3)
5	4	2.5288(6)	0.25(3)	0.60023(2)	0.81840(5)
	6	2.527(1)	0.21(2)	0.60071(4)	0.81400(3)
	8	2.528(2)	0.23(3)	0.60024(5)	0.81007(4)
	10	2.528(4)	0.26(8)	0.5993(2)	0.80831(7)
6	4	2.7701(9)	0.25(3)	0.60350(1)	0.83214(2)
	6	2.7691(9)	0.19(2)	0.60372(4)	0.82709(2)
	8	2.769(3)	0.20(5)	0.60302(8)	0.82384(3)
	10	2.769(3)	0.14(4)	0.6032(2)	0.82562(7)
8	4	3.1968(8)	0.26(4)	0.60654(1)	0.84694(2)
	6	3.196(2)	0.22(4)	0.60673(3)	0.84207(2)
	8	3.197(3)	0.25(7)	0.60633(6)	0.83881(3)
	10	3.192(4)	0.2(1)	0.6040(2)	0.83781(3)

**Table 1:** Values of the bare anisotropy coupling  $\gamma_{\text{np}}$  associated with the renormalised anisotropy  $\xi$ , from numerical simulations of massless  $U(3)$  lattice QCD on  $(\xi N_s) \times N_s^3$  lattices. Also, the corresponding values of the running anisotropy (derivative), the helicity modulus  $a^2 Y$ , and the chiral susceptibility density  $N_s^{-4} a^6 \chi$ . The quantity  $\gamma_{\text{np}}$  exhibits small finite-volume corrections, and is consistent (within errors) with its thermodynamic limits, even on the smallest lattices. This rapid convergence justifies using small-lattice measurements as thermodynamic estimators for  $\gamma_{\text{np}}$ . This is particularly useful in simulations at large  $\xi$ , for which significant statistics can only be obtained on small volumes.

$\xi$	$N_s$	$\gamma_{\text{np}}$	$\frac{\xi}{\gamma} \frac{d\gamma}{d\xi} \Big _{\gamma_{\text{np}}}$	$a^2 Y$	$N_s^{-4} a^6 \chi$	avg. sign
1/2	8	0.5743(2)	0.43(1)	0.27445(2)	0.283426(6)	0.9966(0)
	12	0.5745(2)	0.450(6)	0.274508(6)	0.282272(4)	0.9833(1)
	16	0.5744(2)	0.437(6)	0.274416(6)	0.281835(2)	0.9475(7)
	20	0.5744(4)	0.43(2)	0.274471(7)	0.281641(4)	0.818(4)
	24	0.5747(6)	0.44(2)	0.27461(3)	0.28151(2)	0.64(2)
2/3	6	0.7324(2)	0.405(6)	0.340328(9)	0.362517(3)	0.99863(2)
	12	0.7327(3)	0.38(1)	0.34040(2)	0.359782(8)	0.9777(4)
1	4	0.99993(5)	0.356(2)	0.432995(9)	0.489211(1)	0.991260(3)
	6	1.0000(3)	0.36(2)	0.43384(2)	0.485553(5)	0.99830(2)
	8	1.0002(3)	0.36(2)	0.43400(1)	0.483803(6)	0.99543(7)
	10	0.9999(3)	0.369(5)	0.433984(8)	0.483086(6)	0.9876(2)
3/2	4	1.3117(2)	0.310(5)	0.510010(1)	0.610195(3)	0.996258(6)
	8	1.3116(5)	0.30(2)	0.51025(2)	0.603966(9)	0.9933(2)
2	4	1.5573(2)	0.291(5)	0.548483(6)	0.683099(3)	0.998044(7)
	6	1.5570(4)	0.28(2)	0.54881(2)	0.678484(8)	0.99817(3)
	8	1.5568(6)	0.29(2)	0.54884(2)	0.67668(1)	0.9917(2)
	10	1.5569(6)	0.28(2)	0.54873(3)	0.67564(2)	0.9708(8)
	12	1.5572(6)	0.25(2)	0.54871(2)	0.67517(2)	0.942(3)
3	4	1.9449(2)	0.263(4)	0.581568(4)	0.760045(5)	0.999186(4)
	6	1.944(1)	0.31(6)	0.58201(3)	0.75511(2)	0.99785(8)
	8	1.944(2)	0.32(5)	0.58200(3)	0.75325(2)	0.99205(4)
	10	1.945(1)	0.26(2)	0.58169(5)	0.75144(3)	0.978(2)
4	4	2.258(6)	0.262(9)	0.59431(2)	0.79685(2)	0.999682(4)
	6	2.258(9)	0.27(2)	0.59455(3)	0.79165(2)	0.99885(5)
	8	2.258(2)	0.24(3)	0.59432(5)	0.78910(4)	0.9965(2)
	10	2.257(1)	0.31(3)	0.59474(3)	0.78866(2)	0.984(2)
5	4	2.5288(6)	0.25(3)	0.600(2)	0.81780(2)	0.99974(1)
	6	2.527(1)	0.21(2)	0.6007(5)	0.81290(3)	0.99885(7)
	8	2.5284(2)	0.23(3)	0.6002(6)	0.81010(4)	0.9983(2)
	10	2.528(3)	0.22(5)	0.5993(2)	0.8079(2)	0.954(4)
6	4	2.7701(9)	0.25(3)	0.60350(4)	0.83095(2)	0.99977(1)
	6	2.7691(9)	0.19(2)	0.60372(4)	0.82584(3)	0.999950(6)
	8	2.769(3)	0.20(5)	0.60303(9)	0.8229(2)	0.9964(3)
	10	2.769(2)	0.20(6)	0.60323(7)	0.8215(8)	0.976(3)
8	4	3.1968(9)	0.26(4)	0.60654(6)	0.84591(2)	0.999846(6)
	6	3.196(2)	0.22(4)	0.60673(4)	0.84033(2)	0.99949(4)
	8	3.197(3)	0.25(7)	0.60634(7)	0.83703(8)	0.9970(3)
	10	3.194(4)	0.19(9)	0.6038(2)	0.8352(3)	0.978(3)

**Table 2:** Values of the bare anisotropy coupling  $\gamma_{\text{np}}$  associated with the renormalised anisotropy  $\xi$ , from numerical simulations of massless  $SU(3)$  lattice QCD on  $(\xi N_s) \times N_s^3$  lattices. Also, the corresponding values of the running anisotropy (derivative), the helicity modulus  $a^2 Y$ , the chiral susceptibility density  $N_s^{-4} a^6 \chi$ , and the average baryonic sign. The quantity  $\gamma_{\text{np}}$  exhibits small finite-volume corrections, and is consistent (within errors) with its thermodynamic limits, even on the smallest lattices. This rapid convergence justifies using small-lattice measurements as thermodynamic estimators for  $\gamma_{\text{np}}$ . This is particularly useful in simulations at large  $\xi$ , for which significant statistics can only be obtained on small volumes. In the continuous time limit, the baryons becomes increasingly static, which explains the lack of fluctuations that contribute to the sign problem at large  $\xi$ .

$\xi$	$am_B$
1	2.872(8)
2	1.626(4)
3	1.126(2)
4	0.859(2)
5	0.695(2)
6	0.584(1)

**Table 3:** Values of the static baryon mass  $am_B$  as a function of the anisotropy coupling, from numerical simulations of massless  $SU(3)$  lattice QCD, using a “snake algorithm” [15].